Transition-Edge Sensor Spectrometer for Precision Spectroscopy of Antiprotonic Atoms

Kelsey Morgan, Toshiyuki Azuma, Gonçalo Baptista, Daniel Becker, Douglas Bennett, *Member, IEEE*, François Butin, Jonathan W. Dean, Ofir Eizenberg, Joseph W. Fowler, Hiroyuki Fujioka, Davide Gamba, Johnathon D. Gard, Nabil Garroum, Mauro Guerra, Tadashi Hashimoto, Takashi Higuchi, Masaki Hori, Paul Indelicato, Mark Keller, Jorge Machado, John A.B. Mates, Nathan Nakamura, Jason Nobles, François Nez, Ben Ohayon, Shinji Okada, Nathan Ortiz, Shikha Rathi, Michael Roosa, Jean-Yves Roussé, Takeshi Saito, Daniel Schmidt, Quentin Senetaire, Jonas Sommerfeldt, Paul Szypryt, Joel Ullom, Joel Weber, Pauline Yzombard, Marco Zito, Nancy Paul, and Daniel Swetz

***Abstract*—antiProtonic Atom X-ray (PAX) spectroscopy is an experiment that aims to test strong-field quantum electrodynamics (QED) effects by performing high-precision X-ray spectroscopy of antiprotonic atoms. PAX will use a low-energy antiproton beam provided by the Extra Low ENergy Antiproton (ELENA) ring at the European Organization for Nuclear Research (CERN) to create antiprotonic atoms. A superconducting transition-edge sensor (TES) spectrometer will be used to measure the energy of transitions between circular Rydberg states in these atoms. The energy range of interest for the experiment spans 50 keV to 250 keV, and the desired precision for measuring the centroids of the emission lines is 10^{-5}. The spectrometer for PAX is intended to have four 96-pixel TES arrays and will be read out with a microwave superconducting quantum interference device (SQUID) multiplexer. As a step toward building the full instrument, we built a scaled-down version of the spectrometer that was installed at the TEst Line for Machine And Antimatter eXperiments (TELMAX) facility at ELENA in April 2025. The purpose of this deployment was to make an observation of X-ray emission by antiprotonic atoms and to better understand the effect of the pionic charged particle background due to antiproton annihilation on the performance of the TES array. This pilot spectrometer had an array of 60 TES pixels in a compact adiabatic demagnetization refrigerator cryostat. The sensors were read out with a microwave SQUID multiplexer. Each pixel consisted of a molybdenum/gold bilayer TES with a coplanar gold "landing pad" for a bulk tin absorber that was attached by an epoxy joint. We discuss the design of the TES pixels, the microwave SQUID readout, and the cryogenic platform. Finally, we present calibration data obtained at TELMAX using radioactive sources to assess the performance of the spectrometer in the antiproton beam-OFF condition.**

***Index Terms*—Antiprotonic atoms, quantum electrodynamics (QED), superconducting microcalorimeter, transition-edge sensor (TES).**

I. Introduction

QUANTUM electrodynamics (QED) is one of the best understood field theories, and therefore provides a promising path for searching for new physics beyond the Standard Model [1]. For low-Z systems like the hydrogen atom, it is possible to perform extremely high-precision bound-state QED (BSQED) calculations. Comparisons with laser-spectroscopy experiments have shown agreement at the level of 12 significant digits [2], [3]. There is strong motivation to test BSQED theory at higher-Z and more tightly bound orbitals where electromagnetic field strengths can approach or exceed the Schwinger limit, $\sim 1.32 \times 10^{18}$ Vm^{-1} [4]. This fundamentally changes the theoretical approach, as the interaction with the Coulomb field can no longer be treated in perturbation theory and all-order BSQED calculations must be performed in this strong field regime.

The antiProtonic Atom X-ray spectroscopy (PAX) experiment will use a superconducting transition-edge sensor (TES) spectrometer to measure the photons created from transitions between circular Rydberg states in antiprotonic atoms. Antiprotons are roughly 1836 times heavier than electrons [5] resulting in significantly reduced orbital radii, and therefore increased field strengths where QED effects are enhanced. Moreover, outer shell Rydberg orbitals (high n and maximum allowed l quantum numbers) have minimal dependence on nuclear effects, which may otherwise mask the impact of subtle second-order BSQED effects [6]. This allows PAX to probe different areas of parameter space from other studies that have measured exotic atom transitions, such as the HEATES (muonic and kaonic atoms [7], [8]), and SIDDHARTA-2 (kaonic atoms [9]) collaborations. PAX will provide up to two orders of magnitude better resolution relative to previous studies of antiprotonic atoms that used high-purity

Received 25 September 2025; revised 13 February 2026; accepted 2 March 2026. Date of publication 9 March 2026; date of current version 6 April 2026. This work was supported in part by The PAX Project through ANR Young Researcher Grant in 2023 to 2024 under Grant ANR-23-CE30-0002, in part ERC Starting Grant from 2024 to 2029 under Grant Agreement 101115849, in part by the European Union's Horizon Europe Research and Innovation Programme under Grant Agreement 101057511, and in part by FCT (Portugal) through Research Center Grant under Grant UIDB/FIS/04559/2025 (LIBPhys). The work of Kelsey Morgan, Douglas Bennett, Joseph W. Fowler, Mark Keller, John A.B. Mates, Nathan Nakamura, Nathan Ortiz, Daniel Schmidt, Joel Ullom, and Daniel Swetz was supported by the National Institute of Standards and Technology. The work of Jonathan W. Dean and Paul Szypryt was supported by the U.S. Department of Commerce, National Institute of Standards and Technology through financial assistance award under Grant 70NANB23H027. The work of Takashi Higuchi was supported by the Future Development Funding Program of Kyoto University Research Coordination Alliance and the Itoh Science Foundation. *(Corresponding author: Kelsey Morgan.)*

Please see the Acknowledgment section of this article for the author affiliations.

Color versions of one or more figures in this article are available at https://doi.org/10.1109/TASC.2026.3672351.

Digital Object Identifier 10.1109/TASC.2026.3672351

germanium detectors [10]. The increased resolution will allow tests of second-order BSQED, such as vacuum polarization and self-energy, enabling new studies in fundamental physics.

In addition to the X-rays produced by the antiprotonic atom cascade, there will be a significant background of charged particles due to the annihilation of the antiprotons. The annihilation of low-energy (hundreds of keV) antiprotons with a nucleus produces multiple pions with MeV-scale energies [11]. The pions decay, producing gammas and other charged particles. The pions and/or their decay products will pass through and deposit energy in the sensors.

Installation of the spectrometer is scheduled to occur at the Extra Low Energy Antiproton (ELENA) ring at CERN in 2027. Prior to this deployment, beamtime was given at the TEst Line for Machine and ANtimatter eXperiments (TELMAX) beam line, also at ELENA. This is the first time that the TELMAX facility has been used. The purpose of this pilot experiment is 1) to test the capabilities of TES spectrometers in antimatter experiments, 2) to observe any other systematic issues to be resolved, and 3) to determine whether changes should be made to the TES pixels or other aspects of the experimental setup before the full-scale instrument (four arrays of 96 TES pixels) is built. To this end, we built a scaled-down version of the spectrometer with an array of 60 TES pixels in a compact, portable cryostat.

This work describes the design of the 60-pixel TES spectrometer, the supporting multiplexed readout, and the cryogenics used. Data taken with the calibration sources are presented, i.e., without the antiproton beam, and the performance of the detectors is discussed.

II. TES Spectrometer Design

A. TES Design

A TES is a superconducting thin film that is electrically biased into its superconducting-to-normal transition, where the resistance is a sharp function of temperature. When energy from an incident photon heats the film, the change in resistance can be measured to determine the energy of the photon. Since the TES must be relatively thin (e.g., hundreds of nanometers) in order to achieve the low critical temperatures necessary for high performance [12], [13], it must be thermally coupled to a larger block of high-Z material in order to efficiently detect X-rays with energies up to 250 keV [14].

In our design, each TES "pixel" consists of a molybdenum/gold bilayer TES thermometer thermally coupled to a tin photon absorber. The TES bilayer consists of a 46 nm thick molybdenum layer under a 425 nm thick gold layer. The gold is lithographically patterned into a 30 μm $\times$ 90 μm rectangle, and the molybdenum is patterned into two parallel strips, with opposite ends starting at 12 μm wide and each tapering to 5 μm wide. The gold proximitizes the molybdenum to reduce to critical temperature (T_c) of the structure. The array of 60 sensors has $T_c = (112 \pm 2)$ mK. This critical temperature was chosen in order to be compatible with a base temperature of 80 mK while maintaining ΔE $<$ 100 eV full width at half maximum (FWHM) at 100 keV.

The TES thermometer sits next to a 1.25 mm $\times$ 1.25 mm $\times$ 500 nm patch of gold that acts as a landing pad for a tin photon absorber. The TES and gold pad are thermally connected via a small gold bridge. They are fabricated on a 380 μm thick silicon wafer. Finally, a 1.3 mm $\times$ 1.3 mm $\times$ 0.5 mm tin absorber is epoxied to the gold pad with Stycast 1266 adhesive. To slow down the thermal response time of the pixel and make it compatible with the microwave superconducting quantum interference device (SQUID) multiplexer readout, the thermal conductivity between the pixel and the thermal bath is reduced by etching two 1500 μm $\times$ 50 μm legs into the silicon to suspend the TES and absorber structure. A computer-aided design (CAD) drawing of the pixel design is shown in Fig. 1(a). The calculated expected thermal conductivity between the pixel and the bath is 2.7 nW/K at 100 mK. Measurements of the TES current–voltage curves in test structures yielded a value of G(100 mK) = 2.94 nW/K, very close to the design value. The array consists of 60 identical TES pixels arranged in a grid on a 2 mm pitch on a 20 mm $\times$ 20 mm chip. A drawing of the array layout is shown in Fig. 1(b).

B. Multiplexed Readout

The 60 TES pixels in the array are read by microwave multiplexing of SQUID amplifiers [15]. Each TES is inductively coupled to an rf-SQUID, which is in turn inductively coupled to a superconducting resonator. All the sensors can be read out simultaneously by designing each resonator to have a unique resonant frequency and coupling them to a common microwave feedline [16].

Each of the superconducting resonators has a bandwidth of 300 kHz. We apply a flux ramp with amplitude equal to two flux quanta to each RF SQUID to linearize their response, which limits the maximum sampling rate to 62.5 kHz [17]. There are a total of 112 resonators with their resonant frequencies from 5.58 to 6.05 GHz. The resonators outnumber the TES pixels because the chip designs were originally created to support a sensor array with more pixels. The inputs to the RF SQUIDs were left open on the unneeded resonator/SQUID pairs.

C. Cold Detector Package

The TES array, shunt resistors, and inductor coils for biasing the TESs, and microwave SQUID multiplexer chips are all mounted on a "microsnout" package and cooled to 80 mK. The microsnout is a copper frame designed to hold the chips and the RF and DC connectors that bring signals into and out of the detector package. The TES array is mounted on the top of the microsnout, and the TES bias circuitry and multiplexer chips are mounted on the sides in order to make the entire object more compact. A photograph of the assembled microsnout detector package is shown in Fig. 2.

D. Cryogenics

The detectors and readout are cooled using a cryogen-free two-stage adiabatic demagnetization refrigerator cryostat [18]. The cryostat's two salt pills are gadolinium gallium garnet, which reaches a minimum temperature of $\sim$ 0.5 K, and ferric ammonium alum (FAA), which reaches a minimum temperature of $\sim$ 0.05 K. The TES array and microwave multiplexer chips

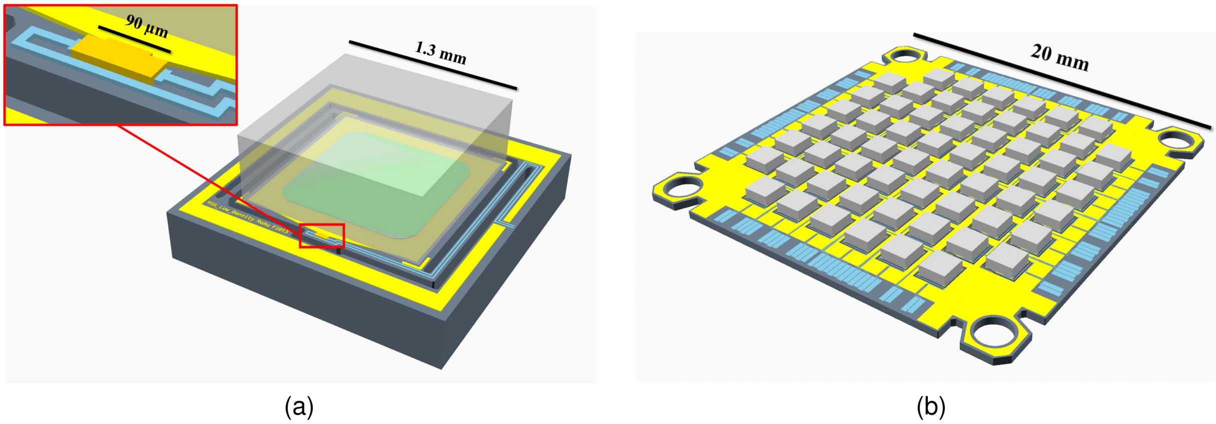

Fig. 1. CAD models of the TES pixel and array layout. (a) Single pixel. The tin absorber is shown semitransparent so that the underlying gold pad (yellow) and the epoxy (green) are visible. A zoomed-in view of the TES, which sits next to the absorber, is shown in the inset highlighted by a red box. The Mo/Au TES bilayer (gold) is 30 μm × 90 μm. Bias current is carried to the TES by 10 μm wide Mo leads (blue). The TES and absorber sit on a 380 μm thick Si island (dark gray), defined by deep etching two long “legs” through the silicon to create a weak thermal connection to the thermal bath. (b) The array contains 60 TES pixels with a 2 mm × 2 mm pitch. The size of the chip is 20 mm × 20 mm. Wire bond pads around the edges of the chip (blue) are used to carry the TES bias in and out. Gold is deposited on the unused surface area of the array (yellow) to improve thermal conductance and provide a surface to add gold bonds for heat sinking to the microsnout.

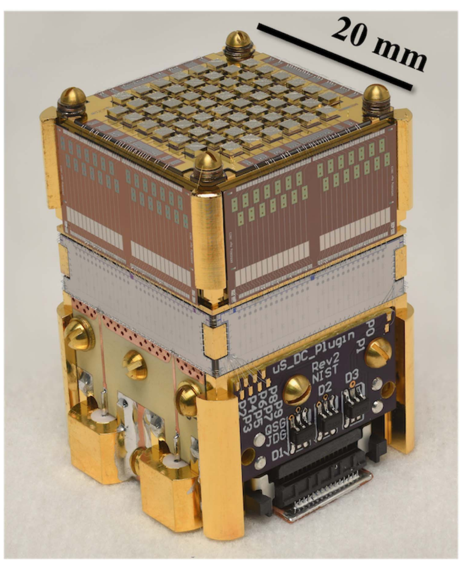

Fig. 2. Microsnout. The 60-pixel TES array is mounted on the top, and around-the-corner wirebonds are used to send bias voltage to the sensors. The TES bias circuitry and microwave multiplexer chips are mounted to the sides of the snout to make the focal plane more compact.

are thermally heat sunk to the FAA stage, which was temperature regulated at 80 mK. With the TESs biased and the microwave readout operating, the hold time was between 16 h and 20 h, depending on the details of the magnet cycle. Recycling the cryogenics by ramping the superconducting magnet took 2 h from the start of the ramp to the time the FAA stage reached the base temperature. So, cycling the magnet twice a day allowed the spectrometer to be ready to acquire data about 80% of the time.

The TESs and SQUIDs are sensitive to magnetic fields of the order of the Earth’s field, and so must be shielded. We used two cylindrical shields made of metal with high magnetic permeability at cryogenic temperatures that were heat sunk to the 3 K and

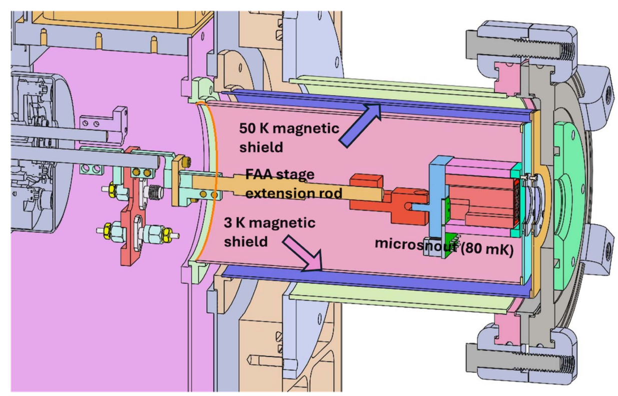

Fig. 3. Mounting and shielding for the detector package. The microsnout is attached to the gold rod that extends from the FAA stage and is temperature regulated to 80 mK. There are two layers of magnetic shielding mounted to the 3 K stage (pink arrow) and 50 K stage (blue arrow) of the cryostat.

50 K stages of the cryostat. To achieve $> 95\%$ transmission for 100 keV photons while maintaining good shielding properties, the 3 K and 50 K shields each have a 17.15 mm diameter aperture that is covered with a thin (50 μm) layer of mu-metal. In addition, the microsnout detector package was enclosed in an aluminum sleeve that also acts as a magnetic shield below the critical temperature of aluminum ($T < 1.2$ K). A drawing showing a cutaway view of the detector package mounting and magnetic shielding is shown in Fig. 3.

E. Installation at TELMAX

The instrument was installed at TELMAX in April 2025. After a four-week commissioning period, the first two-week science run with the antiproton beam began on 5 May 2025.

The experimental setup requires impinging the 100 keV antiproton beam from ELENA onto a target material, and detecting the emitted X-rays from the antiprotonic atom cascade with the TES spectrometer. While the final physics program will use

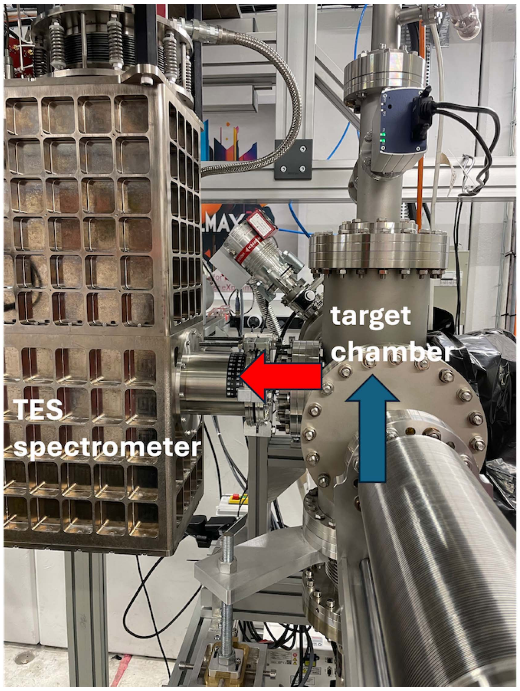

Fig. 4. TES spectrometer (left) and target chamber (right) at TELMAX. The antiproton beam enters through a beam pipe in the floor, traveling upward as indicated by the blue arrow. The antiprotons interact with the target, emitting X-rays isotropically. A titanium window on the target chamber aligns with the aluminum window on the face of the TES spectrometer so that X-rays can be detected by the TES, as indicated by the red arrow.

Fig. 5. Radioactive calibration source attached to the end of the TES spectrometer. The source itself consists of radioactive material distributed on a plastic film, labeled with "PTB" in blue text. The plastic film is mounted in a 3D-printed white plastic holder. In normal operation with the antiproton beam, the calibration source will be between the aluminum window on the face of the TES spectrometer and the titanium window on the target chamber to provide continuous calibration data.

gas targets in order to better probe QED effects [19], for this first test beam run the targets were solid samples mounted on a translating ladder housed in an ultra-high vacuum chamber with a titanium window to allow X-rays to exit the chamber. The TES spectrometer was positioned next to the chamber, with an air gap between the window on the chamber and the 0.254 mm thick aluminum window on the vacuum jacket of the cryostat. The cryostat was suspended from two rails with slides to translate it in one dimension that allowed us to vary the distance between the TES and the target. A photograph of the target chamber and spectrometer is shown in Fig. 4.

Calibration sources for the TES spectrometer were made at Physikalisch-Technische Bundesanstalt (PTB) in Germany by depositing small quantities of radioactive material in drops distributed over a 50 mm diameter circle on a plastic film. The films were mounted in a custom plastic holder that could be attached to the outside of the cryostat's vacuum jacket to position them directly in front of the TES array, while still allowing the photons of interest to pass easily through the thin plastic film (estimated 99.8% transmission for 50 keV photons). A photograph of the calibration sources mounted on the cryostat is shown in Fig. 5.

III. Spectrometer Performance

After installation at TELMAX, the performance of the spectrometer was characterized using radioactive sources ^{57}Co, ^{133}Ba, and ^{152}Eu. These sources were chosen because they produce bright emission lines in the same energy range as the antiprotonic X-rays of interest, from about 50 to 150 keV.

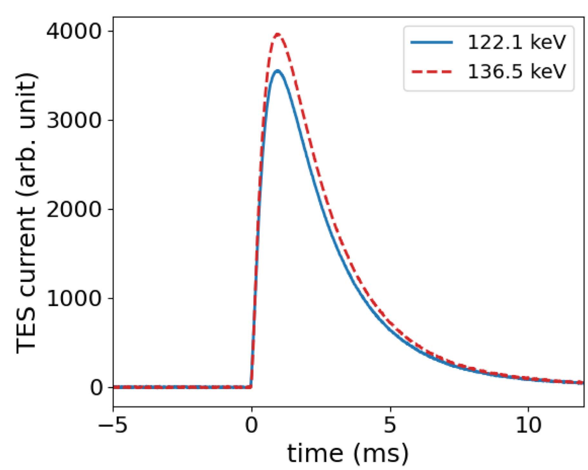

Fig. 6. Example of the pulse response of a single TES pixel to 122.1 keV (blue) and 136.5 keV (red) emission from a ^{57}Co source. The traces shown are single photon absorption events (not averages). This particular sensor had 68 eV FWHM energy resolution at 122.1 keV, which is typical for the array.

An example of the TES response to photons emitted by a ^{57}Co source is shown in Fig. 6. The response time of the TES is an important parameter for the experiment. Because it is a thermal detector, a TES cannot distinguish between two photons (or particles) that arrive simultaneously. To accurately analyze the energy of an event, a pulse must be separated from subsequent events by at least several decay time constants [20], [21]. So, when multiple photons/particles arrive too close in time, those events are discarded. The typical cycle at ELENA produces a 100

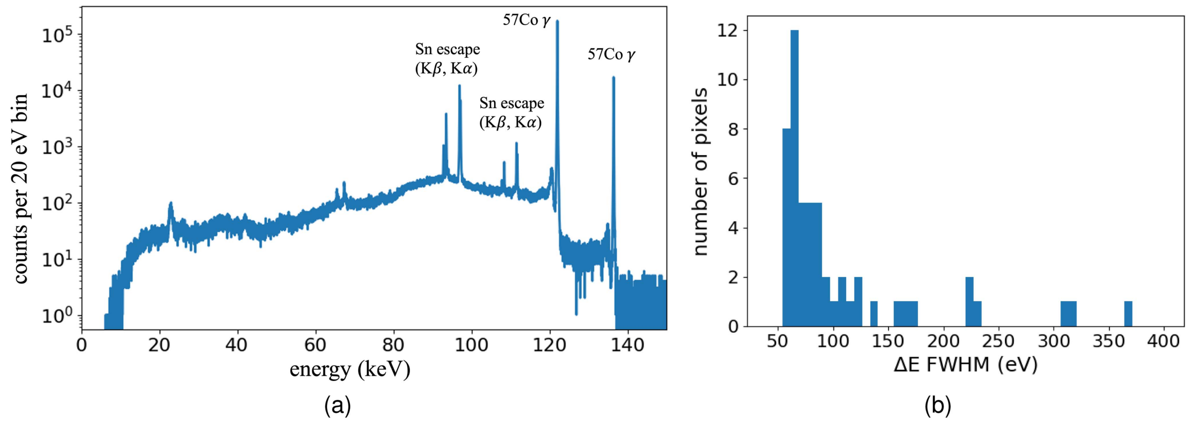

Fig. 7. (a) Emission spectrum of ^{57}Co, coadded for 53 TES pixels. The bright lines at 122.1 and 136.5 keV are gamma rays emitted by ^{57}Co [23]. The lines between 90 and 115 keV are escape peaks, which occur when an incident gamma ray from the ^{57}Co excites a tin Kα or Kβ X-ray that leaves the absorber. (b) Histogram of the energy resolution of the individual pixels in the array at 122.1 keV.

ns long bunch of $\sim 10^7$ antiprotons every 2 min. However, we found that in this mode, the rate of events on the detector (signal X-rays plus charged particle background) was $>>1$ event per sensor per antiproton bunch. In fact, the total energy deposited on the detector was so high that it caused brief 100 μK-scale temperature increases from the 80 mK cold stage when the antiproton bunches arrived, whereas typically the temperature was controlled to within 10 μK rms.

Therefore, we split the antiproton bunches to reduce the instantaneous flux on the detector and to increase the antiproton bunch repetition rate (a similar example with protons is described in [22]). In the end, the antiproton beam at TELMAX was delivered to the target chamber in short (<1 μs) bunches with 100 ms spacing. Groups of 100 to 200 bunches were delivered over the course of 10 s to 20 s, and that pattern repeated every 2 min. In addition, the bunch intensity was reduced from the maximum available. With the TES detector positioned approximately 28 cm from the target, this resulted in a rate of $\sim$2.6 counts per second per sensor (including background events) averaged over the course of a 10 s spill. In addition, a radioactive source was used to continuously monitor the gain of the sensors between the arrival of antiproton bunches.

In the split bunch operating mode, the TES pulse length should be short compared to the 100 ms bunch repetition rate to avoid dead time. For the 53 working sensors in the array, the exponential decay time constant of the pulses was 1.84 ms on average with a standard deviation of 0.37 ms across the sensors. The sensor-to-sensor variation is a result of small variations in the critical temperature of the sensors and variation in the bias resistors.

Analysis of the performance of the detector with the antiproton beam ON is ongoing. Here, we report the performance of the TES array with the beam OFF. The energy resolution of the array was measured using a ^{57}Co source. The median resolution of the 53 working sensors at 122.1 keV was 76.3 eV FWHM. The emission spectrum of ^{57}Co for all sensors coadded and a histogram of the energy resolution for all sensors are shown in Fig. 7. The bright peaks at 122.1 and 136.5 keV are gamma rays emitted by ^{57}Co. The peaks at 93.6, 97.0, 108.0, and 111.2 keV are escape peaks, where the incident gammas from the source excite a Kα or Kβ X-ray from the tin absorber that then escapes from the absorber.

IV. Conclusion and Future Work

We have designed a TES spectrometer and installed it at the TELMAX antimatter beamline at CERN. The spectrometer was used to measure the X-ray emission from antiprotonic atoms formed from antiprotons incident on solid targets. The purpose of this initial experiment is to benchmark the detector's performance and to compare with previous measurements of antiprotonic X-rays made with solid-state detectors.

The spectrometer achieved 76.3 eV FWHM median energy resolution at 122.1 keV for 53 TES pixels at TELMAX in the antiproton beam-OFF state. The TES pulse length was compatible with the 100 ms repetition rate of the antiproton bunches from ELENA. When the beam was turned ON, the intensity of the antiproton bunches was sufficient to produce > 1 event per sensor per bunch if the TES was positioned as close as possible to the target chamber.

The observed event rates has implications for the design of the final instrument. Since the signal rate is not limited by the brightness of the source but rather by the need to avoid pileup, upgrades to the instrument should prioritize adding more pixels to the array. Therefore, our goal for the final instrument is to deploy four arrays of 96 pixels using the same microsnout detector package, which will increase statistics (or reduce measurement time) by a factor of 6.4. To fit 96 pixels into the same 20 mm $\times$ 20 mm array footprint, we are considering two detector designs. A 1 mm $\times$ 1 mm $\times$ 1 mm tin absorber would preserve the total detector volume (and therefore the energy range and energy resolution), but would allow us to fit 96 pixels into the available area. Alternatively, we are testing methods of etching a pillar structure into the current 1.3 mm $\times$ 1.3 mm $\times$ 0.5 mm absorbers that would suspend most of the absorber area above the substrate. The TES and wiring can then be placed under the overhanging portion of the absorber. This design enables closer pixel-packing, which could reduce crosstalk caused by events that strike the silicon substrate between pixels.

The initial measurements with the antiproton beam were made in May 2025 and the results of these measurements will be the subject of a future publication. In addition to measurements of antiprotonic X-rays, this spectrometer will provide valuable information about the performance of the TES in the presence of a charged particle background due to antiproton annihilation, which will be fed back into the design of the larger-area TES array that will be deployed to ELENA in 2027.

IV. Disclaimer

Certain equipment, instruments, software, or materials are identified in this paper in order to specify the experimental procedure adequately. Such identification is not intended to imply recommendation or endorsement of any product or service by NIST, nor is it intended to imply that the materials or equipment identified are necessarily the best available for the purpose.

Acknowledgment

The authors would like to thank Dr. Ali Eichenberger for his kind assistance in fabricating holders for the radioactive calibration sources on short notice.

Authors' Affiliations

Kelsey Morgan, Douglas Bennett, Joseph W. Fowler, Mark Keller, John A.B. Mates, Nathan Nakamura, Nathan Ortiz, Daniel Schmidt, and Daniel Swetz are with the National Institute of Standards and Technology, Boulder, CO 80305 USA (e-mail: kelsey.morgan@nist.gov).

Toshiyuki Azuma and Takeshi Saito are with the RIKEN Laboratory, WPI-QUP, KEK, Ibaraki 305-0801, Japan.

Gonçalo Baptista, Paul Indelicato, François Nez, Michael Roosa, Quentin Senetaire, Jonas Sommerfeldt, Pauline Yzombard, and Nancy Paul are with the Laboratoire Kastler Brossel, Sorbonne Université, CNRS, ENS-PSL Research University, Collège de France, F-75005 Paris, France.

Daniel Becker, Johnathon D. Gard, Jason Nobles, Paul Szypryt, and Joel Weber are with the Department of Physics, University of Colorado Boulder, Boulder, CO 80309 USA.

François Butin and Davide Gamba are with the CERN, Meyrin, 1217 Genève, Switzerland.

Jonathan W. Dean and Joel Ullom are with the National Institute of Standards and Technology, Boulder, CO 80305 USA, and also with the University of Colorado Boulder, Boulder, CO 80309 USA.

Ofir Eizenberg and Ben Ohayon are with the Technion–Israel Institute of Technology, Haifa 3200003, Israel.

Hiroyuki Fujioka is with the Institute of Science Tokyo, Tokyo 152-8551, Japan.

Nabil Garroum and Marco Zito are with the Laboratoire de Physique Nucléaire et des Hautes énergies, 75252 Paris, France.

Mauro Guerra and Jorge Machado are with the LIBPhys-UNL, NOVA University Lisbon, 2829-516 Caparica, Portugal.

Tadashi Hashimoto is with the RIKEN Nishina Center, RIKEN, Wako 351-0198, Japan.

Takashi Higuchi is with the Kyoto University, Osaka 606-8501, Japan, and also with the The University of Osaka, Osaka 565-0871, Japan.

Masaki Hori is with the Department of Physics, Imperial College London, SW7 2AZ London, U.K., and also with the Max Planck Institute of Quantum Optics, 85748 Garching, Germany.

Shinji Okada is with the Chubu University, Aichi 487-8501, Japan.

Shikha Rathi is with the Technion–Israel Institute of Technology, Haifa 3200003, Israel, and also with the Laboratoire Kastler Brossel, Sorbonne Université, 75230 Paris, France.

Jean-Yves Roussé is with the IRFU, CEA, Université Paris-Saclay, F-91191 Gif-sur-Yvette, France.

References

[1] M. S. Safronova, D. Budker, D. DeMille, D. F. J. Kimball, A. Derevianko, and C. W. Clark, "Search for new physics with atoms and molecules," *Rev. Modern Phys.*, vol. 90, Jun. 2018, Art. no. 025008. [Online]. Available: https://link.aps.org/doi/10.1103/RevModPhys.90.025008

[2] A. Matveev et al., "Precision measurement of the hydrogen $1s{-}2s$ frequency via a 920-km fiber link," *Phys. Rev. Lett.*, vol. 110, Jun. 2013, Art. no. 230801. [Online]. Available: https://link.aps.org/doi/10.1103/PhysRevLett.110.230801

[3] H. Fleurbaey et al., "New measurement of the $1s - 3s$ transition frequency of hydrogen: Contribution to the proton charge radius puzzle," *Phys. Rev. Lett.*, vol. 120, May 2018, Art. no. 183001. [Online]. Available: https://link.aps.org/doi/10.1103/PhysRevLett.120.183001

[4] J. Schwinger, "On gauge invariance and vacuum polarization," *Phys. Rev.*, vol. 82, pp. 664–679, Jun. 1951. [Online]. Available: https://link.aps.org/doi/10.1103/PhysRev.82.664

[5] M. Hori et al., "Buffer-gas cooling of antiprotonic helium to 1.5 to 1.7k, and antiproton-to–electron mass ratio," *Science*, vol. 354, no. 6312, pp. 610–614, 2016. [Online]. Available: https://www.science.org/doi/abs/10.1126/science.aaf6702

[6] G. Baptista et al., "Towards precision spectroscopy of antiprotonic atoms for probing strong-field qed," in *Proc. Int. Conf. Exotic At. Related Topics Conf. Low Energy Antiprotons*, 2025, Art. no. 085.

[7] T. Okumura et al., "Proof-of-principle experiment for testing strong-field quantum electrodynamics with exotic atoms: High precision x-ray spectroscopy of muonic neon," *Phys. Rev. Lett.*, vol. 130, Apr. 2023, Art. no. 173001. [Online]. Available: https://link.aps.org/doi/10.1103/PhysRevLett.130.173001

[8] S. Okada et al., "First application of superconducting transition-edge sensor microcalorimeters to hadronic atom X-ray spectroscopy," *Prog. Theor. Exp. Phys.*, vol. 2016, no. 9, 2016, Art. no. 091D01.

[9] F. Sgaramella et al., "High precision X-ray spectroscopy of Kaonic Neon," *Phys. Lett. B*, vol. 865, 2025, Art. no. 139492.

[10] D. Gotta, K. Rashid, B. Fricke, P. Indelicato, and L. M. Simons, "X-ray transitions from antiprotonic noble gases," *Eur. Phys. J. D*, vol. 47, no. 1, pp. 11–26, 2008.

[11] M. Clover, R. DeVries, N. DiGiacomo, and Y. Yariv, "Low energy antiproton-nucleus interactions," *Phys. Rev. C*, vol. 26, no. 5, 1982, Art. no. 2138.

[12] K. D. Irwin and G. C. Hilton, "Transition-edge sensors," in *Cryogenic Particle Detection*. Berlin, Germany: Springer, 2005, pp. 63–150.

[13] G. Brammertz, P. Verhoeve, R. D. Hartog, and A. Peacock, "Critical temperature of superconducting bilayers: Theory and experiment," *Appl. Phys. Lett.*, vol. 80, no. 16, pp. 2955–2957, 2002.

[14] D. T. Chow, A. Loshak, M. L. van den Berg, M. A. Frank, T. W. Barbee Jr, and S. E. Labov, "High-resolution gamma-ray spectrometers using bulk absorbers coupled to Mo/Cu multilayer superconducting transition-edge sensors," *Gamma-Ray Neutron Detect. Phys. II*, vol. 4141, pp. 67–75, 2000.

[15] J. Mates and K. Lehnert, "Demonstration of a multiplexer of dissipationless superconducting quantum interference devices," *Appl. Phys. Lett.*, vol. 92, no. 2, 2008, Art. no. 2531.

[16] J. Mates et al., "Simultaneous readout of 128 X-ray and gamma-ray transition-edge microcalorimeters using microwave squid multiplexing," *Appl. Phys. Lett.*, vol. 111, no. 6, 2017, Art. no. 062601.

[17] J. A. Mates, K. Irwin, L. Vale, G. Hilton, J. Gao, and K. Lehnert, "Flux-ramp modulation for squid multiplexing," *J. Low Temp. Phys.*, vol. 167, no. 5, pp. 707–712, 2012.

[18] C. Hagmann and P. Richards, "Two-stage magnetic refrigerator for astronomical applications with reservoir temperatures above 4k," *Cryogenics*, vol. 34, no. 3, pp. 221–226, 1994.

[19] N. Paul, G. Bian, T. Azuma, S. Okada, and P. Indelicato, "Testing quantum electrodynamics with exotic atoms," *Phys. Rev. Lett.*, vol. 126, Apr. 2021, Art. no. 173001. [Online]. Available: https://link.aps.org/doi/10.1103/PhysRevLett.126.173001

[20] A. Puiu et al., "Transition-edge sensors for holmes," *J. Low Temp. Phys.*, vol. 199, no. 3, pp. 716–722, 2020.

[21] P. Peille et al., "The performance of the athena X-ray integral field unit at very high count rates," *J. Low Temp. Phys.*, vol. 193, no. 5, pp. 940–948, 2018.

[22] R. Garoby, S. Hancock, and J. Vallet, "Demonstration of bunch triple splitting in the CERN PS," in *Proc. 7th Eur. Particle Accelerator Conf.*, Jun. 2000, p. 304.

[23] M. Bhat, "Nuclear data sheets for a = 57," *Nucl. Data Sheets*, vol. 85, no. 3, pp. 415–536, 1998. [Online]. Available: https://www.sciencedirect.com/science/article/pii/S0090375298900217